NANOSCALE AND MICROSCALE THERMOPHYSICAL ENGINEERING
http://dx.doi.org/10.1080/15567265.2017.1289573

Taylor & Francis
Taylor & Francis Group

Perfect Absorption With Trapezoidal Gratings Made of Natural Hyperbolic Materials

B. Zhao and Z. M. Zhang

G.W. Woodruff School of Mechanical Engineering, Georgia Institute of Technology, Atlanta, Georgia, USA

ABSTRACT

Broadband absorption is needed for a wide spectrum of applications such as solar–thermal conversion, radiative cooling, and photodetection. In this work, we theoretically show that trapezoidal gratings made of a natural hyperbolic material on a metal substrate can be used to achieve omnidirectional perfect absorption in a relatively broad spectral region. Hexagonal boron nitride (hBN) is taken as a mid-infrared polar material with hyperbolic characteristic in the wavelength region from 6.2 to 7.3 μm. The anisotropic rigorous-coupled wave analysis is used to calculate the absorptance as well as the local power dissipation and field distributions. The main mechanism for the broadband perfect absorption is elucidated by considering the slow-light effect in a hyperbolic waveguide, which can trap the incident light of different wavelengths in different regions of the trapezoid. The spectral range and bandwidth of near perfect absorption can be adjusted within the hyperbolic range of the material by changing the shape of the trapezoid. Moreover, the substrate can play a role on the reflectance and transmittance of the structure for the wavelengths that do not support the slow-light effect. Similar designs can be applied to other hyperbolic materials to achieve perfect absorption in various wavelength regions.

ARTICLE HISTORY
Received December 6 2016
Accepted January 27 2017

KEYWORDS
Broadband perfect absorption; gratings; hexagonal boron nitride; hyperbolic materials; slow-light effect

Introduction

Achieving perfect absorption of electromagnetic waves in different wavelength ranges is of critical importance in applications such as energy harvesting, photodetection, chemical sensing, and radiative cooling. Various metamaterials have been proposed to achieve perfect absorption for different applications [1–8]. Most of the absorption spectra show a single resonance peak because the absorption is caused by coherent resonances and thus the bandwidth is still quite narrow even when very lossy materials are used. This can be disadvantageous in some energy harvesting or conversation applications [9, 10]. Significant progress has been made and various structures have been proposed to broaden the absorption spectrum in the visible and infrared range. An intuitive way to achieve a broadband behavior is to pack several coherent resonators with close resonance wavelengths or create different resonance modes in the same structure [11–14]. Such designs have been demonstrated using complex gratings [11], metal/dielectric/metal structures with a cluster of different metal patches as the top layer [12, 15], structures assembled by nanoparticles of different sizes [16], and thin-film silicon sandwiched by trapezoidal surface and silver grating [17]. Because the coupling between resonators or different modes can deteriorate the high absorption, it is difficult to achieve very strong absorption in a broadband. Alternatively, one can use nanowires to achieve

CONTACT Z. Zhang zhuomin.zhang@me.gatech.edu G.W. Woodruff School of Mechanical Engineering, Georgia Institute of Technology, Atlanta, GA 30332, USA.

Current address for B. Zhao: Department of Electrical Engineering, Ginzton Laboratory, Stanford University, Stanford, CA 94305, USA.

Color versions of one or more of the figures in the article can be found online at www.tandfonline.com/mmer.

index matching that results in a broadband absorption by using suitable materials [18–20], though the wavelength range and bandwidth of the absorption spectrum are still limited due to the available material choices. Therefore, exploring new materials and new mechanisms to achieve broadband high absorptance remains an active research field.

Nomenclature

E	electric field, V m^{-1}
h	height, m
i	$\sqrt{-1}$
k	magnitude of wavevector, m^{-1}
t	length, m
v	speed, m s^{-1}
w	local power dissipation density, W m^{-3}
x, y, z	space coordinate, m
Greek Symbols	
γ	scattering rate, rad s^{-1}
ε	relative permittivity (dielectric function)
ε_0	electric permittivity of vacuum, 8.854×10^{-12} Fm^{-1}
ε_∞	high-frequency constant in the dielectric function
ζ	magnitude of wavevector, m^{-1}
Λ	period, m
λ	wavelength in vacuum, m
ν	wavenumber, cm^{-1}
ω	angular frequency, rad s^{-1}
ω_p	plasma frequency, rad s^{-1}
Subscripts	
$\parallel$	out-of-plane or the z-direction
$\perp$	in-plane or the x- or y-direction
b	base
t	top

Hyperbolic materials are a special category of anisotropic media that have metallic behaviors (i.e., negative permittivity) or dielectric behaviors (i.e., positive permittivity) in different directions [21]. Because natural hyperbolic materials are scarce especially in the visible range, previous research has been largely focused on artificially constructed metamaterials such as alternating multilayers of metal and dielectric that can effectively show hyperbolic response [21, 22]. These multilayer metamaterials can enable high absorption in a relatively broad spectral region when sculpted to a tapering sawtooth shape [23–25], indicating a potential way of achieving broadband absorption from hyperbolic responses. Different from the broadband absorption achieved by packing together isolated resonators with close resonance wavelength, the broadband absorption in hyperbolic metamaterials relies on perfect absorption that can theoretically be achieved at continuous wavelengths inside the hyperbolic frequency regions of the materials. The fabrication process is often very challenging, especially in the visible and near-infrared regions, because the deposition and etching of layers of metals and dielectrics need to be precisely controlled at very small length scales [26, 27].

It has been shown that materials with natural hyperbolicity are accessible from the visible to the microwave range [28]. Due to crystalline anisotropy or the layered structures, these materials can exhibit intrinsic hyperbolic dispersion in a certain frequency region. In the present study, we show

that omnidirectional broadband perfect absorption can be attained using trapezoidal gratings made of hexagonal boron nitride (hBN) in the mid-infrared region, where hBN exhibits a type II hyperbolicity. The numerical algorithm based on anisotropic rigorous-coupled wave analysis is used to calculate the absorptance of the structure as well as the local power dissipation and electromagnetic field distributions. The mechanisms of the perfect absorption are elucidated. Furthermore, the effects of the trapezoidal geometric parameters on the bandwidth of the absorptance spectrum are examined.

Proposed structure for perfect absorption

The proposed trapezoidal grating structure is illustrated in Figure 1 using hBN as an example of natural hyperbolic materials to construct the perfect absorber in a relative broad mid-infrared band. The hBN grating is periodic in the x-direction (with a period Λ) and extends to infinity in the y-direction. Each period contains an hBN isosceles trapezoid whose height, short, and long bases are h, t_t, and t_b, respectively. The substrate is made of silver (Ag) and is thick enough to be treated as opaque (semi-infinite). Therefore, the incident light will be either reflected or absorbed, and the absorptance can be indirectly calculated from one minus the reflectivity. Plane waves are incident from vacuum at an incidence angle θ. The plane of incidence is the x–z plane and the magnetic field is polarized in the y-direction, i.e., transverse magnetic (TM) waves. The wavevector of the incident wave can be expressed as $\mathbf{k}_{\text{inc}} = k_0 \sin\theta\ \hat{\mathbf{x}} + k_0 \cos\theta\ \hat{\mathbf{z}}$, where k_0 is the magnitude of the wavevector in a vacuum. The dielectric function of Ag is obtained using a Drude model [29]:

$$\varepsilon(\omega) = \varepsilon_\infty - \frac{\omega_p^2}{\omega(\omega + i\gamma)},$$

where the used parameters are plasma frequency $\omega_p = 1.39 \times 10^{16}\text{rad/s}$, scattering rate $\gamma = 2.7 \times 10^{13}\text{rad/s}$, and high-frequency constant $\varepsilon_\infty = 3.4$. The anisotropic property of hBN is described by a tensor, $\bar{\bar{\varepsilon}}_{\text{hBN}} = \text{diag}(\varepsilon_\perp, \varepsilon_\perp, \varepsilon_\parallel)$, with the optical axis in the z-direction in the given

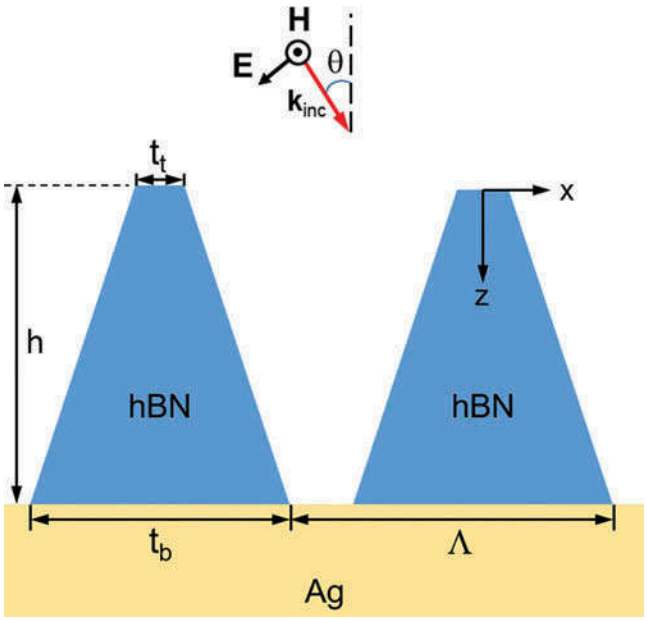

Figure 1. Schematic of the proposed hBN trapezoidal grating structure.

coordinate [30]. The real and imaginary parts of the dielectric function are respectively denoted as ε' and ε'' hereafter. The in-plane transverse and longitudinal optical phonon modes in hBN respectively locate at 1370 and 1610 cm^{-1} and result in a type II hyperbolic region from about 6.2 to 7.3 μm, in which $\varepsilon'_{\perp}<0$ and $\varepsilon'_{\parallel}>0$.

The standard RCWA algorithm was extended to include anisotropic materials [31] and the anisotropic rigorous-coupled wave analysis is employed here to calculate the reflectance as well as electromagnetic field distribution. In the modeling, the incident medium is a vacuum and the substrate is Ag. The hBN trapezoid is discretized into 100 layers in the z-direction in a stairwise manner and thus the thickness of each layer is 100 nm. Each of the layers possesses the same period in the x-direction but a gradually changed filling ratio. In the spectrum calculations, 141 diffraction orders are used to ensure convergence. The field plot is calculated using a total diffraction order of 1001.

The absorption spectrum of the designed structure is displayed in Figure 2 for TM waves with h = 10 μm, Λ = 3 μm, t_t = 0.04 μm, and t_b = 2 μm. The absorptance is close to unity in a relatively broad wavelength range for which hBN exhibits type II hyperbolicity. The sharp drop at the edges of the high absorption range is due to the disappearance of hyperbolicity of hBN and is a prominent difference compared to the absorption spectrum of a coherent resonator. Note that the bandwidth of the perfect absorption achieved using hBN may not be very broad because its hyperbolic region only extends from 6.2 to 7.3 μm. However, the methodology discussed here can be applied to other hyperbolic materials with much broader hyperbolic regions [28] and the maximum bandwidth of the perfect absorption is solely limited by the wavelength range of the hyperbolic region of the material.

The broadband absorptance is insensitive to the incidence direction as demonstrated in Figure 3, unlike the narrowband absorption caused by surface waves such as surface plasmon polaritons [29]. The spectrum maintains its broadband feature omnidirectionally and the absorptance remains higher than 0.8 even at $\theta = 80°$. Furthermore, one may use gratings with hBN pyramids, which is a two-dimensional counterpart of the proposed structure, to obtain broadband

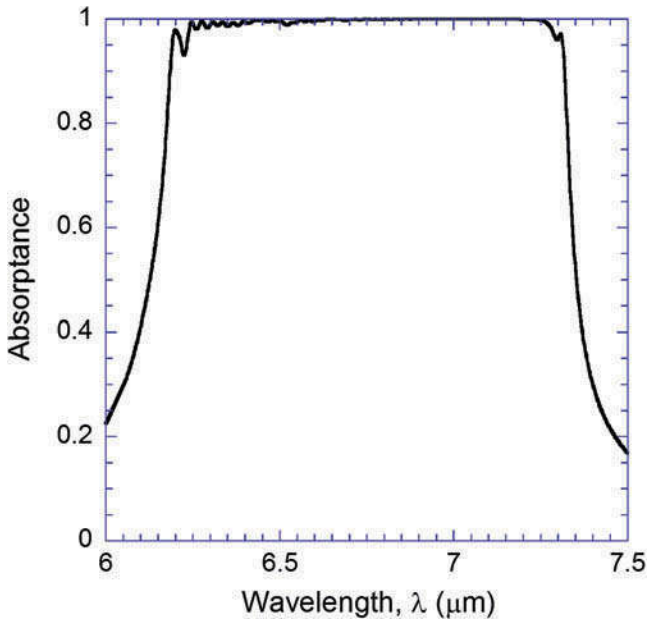

Figure 2. Absorptance spectrum for TM waves at normal incidence ($\theta = 0°$) of the proposed structure (shown in the inset) with hBN trapezoidal gratings on an Ag substrate. The grating parameters are h = 10 μm, Λ = 3 μm, t_t = 0.04 μm, and t_b = 2 μm.

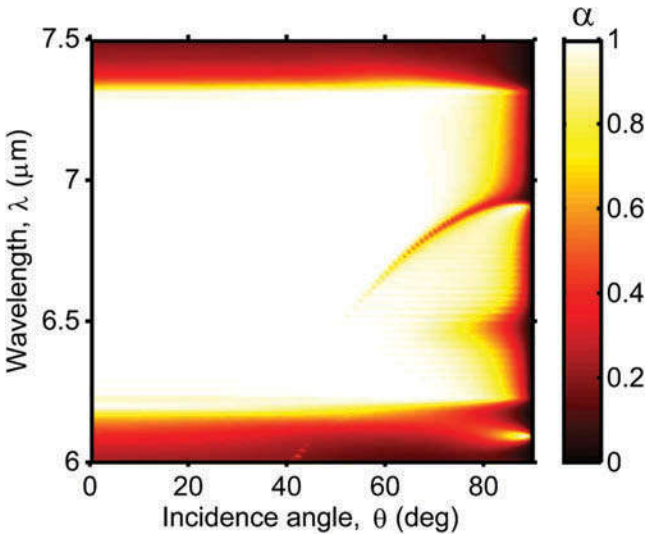

Figure 3. Angular dependence of the broadband absorptance of the trapezoidal grating with the same geometry as the structure shown in Figure 1.

high absorption for both polarizations. One way to fabricate such a structure is to use a template-stripping method by applying Si wafers with inverted pyramids as a template [32], though challenges exist in tuning the geometries of the pyramid. Alternatively, electron beam lithography may be used to directly pattern the grating on a hBN film as has been demonstrated with similar nanocone structures [33, 34].

Discussion of underlying mechanisms

The mechanisms of the broadband absorption can be elucidated by the contour plots in Figure 4. The three columns are for three different wavelengths: λ = 6.63, 7, and 7.2 μm, respectively. The local power dissipation density [31, 35] is calculated based on

$$w(x,z) = \frac{1}{2}\varepsilon_0\omega\left(\varepsilon''_{\perp}|E_x|^2 + \varepsilon''_{\parallel}|E_z|^2\right),$$

where ε_0 and ω are the vacuum permittivity and angular frequency, respectively. The dissipation profile is shown in the upper row. The magnitude of the z-component electric field (E_z) is displayed in the lower row. The absorptance at all three wavelengths is greater than 0.99. At λ = 6.63 μm, the dissipation accumulates mostly at the upper portion of the hBN trapezoid as shown in Figure 4a, indicating that the majority of the power is dissipated therein. When the resonance wavelength becomes longer, the dissipation profile moves toward the bottom of the trapezoid, as shown in Figures 4b and 4c. Note that in the type II hyperbolic region, the major contribution to the dissipation comes from the in-plane losses. For example, at λ = 7 μm, $\varepsilon_{\perp}$ = −16.338 + 0.924i and $\varepsilon_{\parallel}$ = 2.784 + 0.0006i. Therefore, although the in-plane electric field $|E_x|$ in hBN is nearly one order of magnitude smaller compared to $|E_z|$, it can still dominate the contribution to power dissipation w. The distribution of $|E_x|$ in the hBN grating is very similar to that of w and thus is not shown. The distribution of $|E_z|$ is very different because it is higher near the sides than at the center. Though $|E_z|$ appears to be symmetric, the signs are opposite on the left and right sides. The current field inside the grating actually forms loops, as in the case of magnetic polaritons [7]. The dissipation contours show a clear standing wave feature with a relatively longer spatial period toward the lower part of the trapezoid, and the electric field plots echo this pattern well. The absorption in different regions can

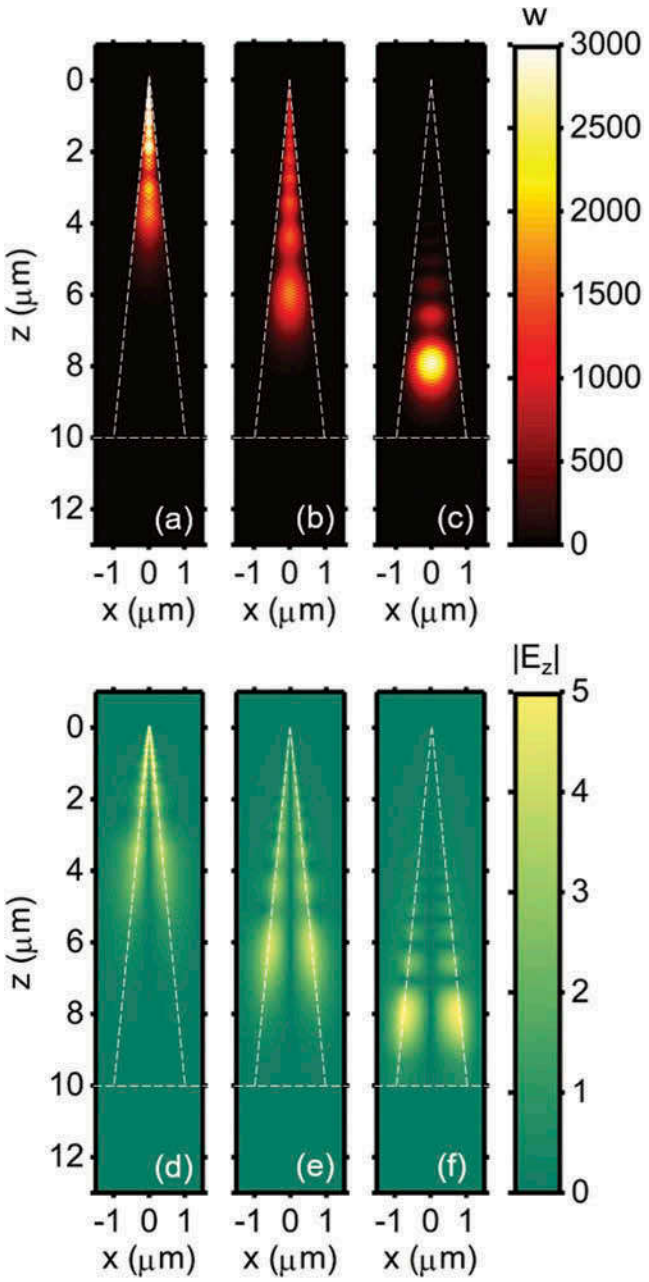

Figure 4. (a)–(c) Local power dissipation density and (d)–(f) *z*-component electric field at three different resonance wavelengths: (Left column) $\lambda = 6.63$ μm or $\nu = 1508$ cm^{-1}, (middle column) $\lambda = 7$ μm or $\nu = 1429$ cm^{-1}, and (right column) $\lambda = 7.2$ μm or $\nu = 1389$ cm^{-1}. Values exceeding 3,000 W/m^3 or 5 V/m are shown in white color. The incidence electric field is 1 V/m. The surfaces of the trapezoids and the Ag substrate are delineated by dashed lines.

be obtained by a volumetric integration of the local power dissipation [31]. It is found that almost all of the power is dissipated within the hBN trapezoid and the absorption by the Ag substrate is less than 1%. The field plots also reveal that the resonances are highly localized, indicating that the coupling between neighboring hBN trapezoids can be neglected. These resonance features are caused by the waveguide modes, to be discussed next.

Considering a waveguide whose core is made of a uniaxial anisotropic material whose dielectric tensor $\bar{\bar{\varepsilon}}$ is described by $\varepsilon_\perp$ and $\varepsilon_\parallel$, as illustrated in Figure 5a, where the cladding material is assumed to be vacuum with a dielectric function $\varepsilon_2 = 1$. The waveguide is infinite long along the z-direction and its width is denoted as t. For TM waves, the dispersion of the waveguide modes can be expressed as

$$\frac{k_{x,2}\varepsilon_\parallel}{k_{x,1}\varepsilon_2} = \tan\left(\frac{k_{x,1}t}{2}\right),$$

where $k_{x,2} = \sqrt{\zeta^2 - \varepsilon_2 k_0^2}$ and $k_{x,1} = \sqrt{\varepsilon_\parallel k_0^2 - (\varepsilon_\parallel/\varepsilon_\perp)\zeta^2}$, with ζ being the z-component of the wavevectors in both regions [24]. Figure 5b shows the dispersion relationship of the fundamental waveguide mode at t = 0.2, 0.6, 1, 1.4, and 1.8 μm when the core material is hBN. Here, the frequency is expressed in terms of wavenumber, $\nu = \omega/(2\pi c_0)$, with c_0 being the light speed in a vacuum. Note that loss is neglected when solving the dispersion curves. The group velocity is along the z-direction and can be obtained from the dispersion curves because $v_g = d\omega/d\zeta$. For a specific core width, the slope of the dispersion curve is positive at small values of ζ, suggesting that a positive group velocity and the power will flow inside the waveguide toward the positive z-direction. However, v_g decreases as ζ increases and becomes zero at maximum of the dispersion curve, beyond which v_g becomes negative. There exists a slow-light effect at the maximum point, where the energy of the wave is trapped inside the waveguide without propagating [23, 24]. Therefore, a hyperbolic waveguide with a specific core width can effectively halt the power flow at a certain wavelength. When t becomes larger, the standing waves will occur at lower frequencies or longer wavelengths.

Because the coupling between neighboring hBN trapezoids is negligible, each trapezoid can be viewed as a waveguide with an increasing core width. For a specific wavelength, the incident wave enters the hBN trapezoid from the narrower end and the power can propagate downward. As the core width becomes larger, v_g decreases gradually as the power flows down. At a certain t, v_g becomes zero and the power is trapped at this location without further flowing due to the slow-light effect. For example, for λ = 6.63 μm (ν = 1508 cm^{-1}), the slow-light effect occurs at t = 1 μm, which matches well with the field plots shown in Figures 4a and 4d where the field stops propagating around halfway of the trapezoid. For λ = 7 μm (ν = 1429 cm^{-1}) and λ = 7.2 μm (ν = 1389 cm^{-1}), the slow-light effect occurs respectively at t = 1.44 and 1.73 μm, also corresponding well to the dissipation contours and field plots in Figure 4. At a specific t, the waveguide supports two modes

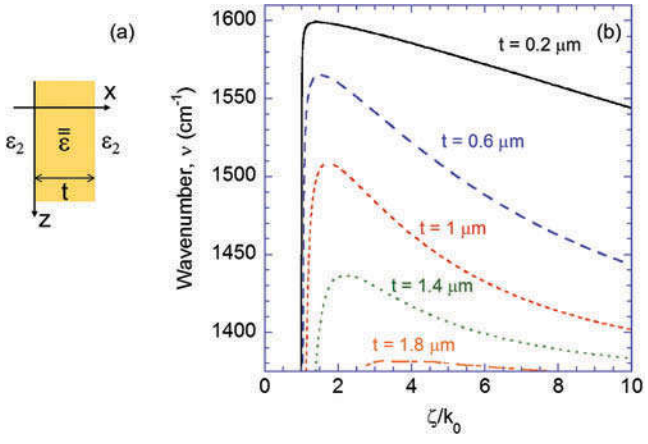

Figure 5. (a) Schematic of an anisotropic waveguide made of a uniaxial material with its optical axis in the z-direction cladded by a dielectric material (ε_2). (b) The dispersion curves of the fundamental waveguide mode in a hyperbolic waveguide with different waveguide widths (t) when the core material is hBN.

with different ζ values. The standing wave patterns are created due to interference effect of these two waves. Because the spatial period of interference patterns is inversely proportional to the difference between the two ζ values, the period is relatively longer near the location that supports slow-light effects where the difference in the two ζ values degenerates to zero [24]. This difference tends to be larger toward the top of the trapezoid where t becomes smaller, resulting in shorter spatial periods therein. Note that because the slow-light effect requires a type II hyperbolicity, the broadband absorption cannot be supported by the proposed grating structure in the type I hyperbolic region (i.e., $\varepsilon'_{\perp}>0$ and $\varepsilon'_{\parallel}<0$), which can also be supported by hBN at longer wavelengths. The phenomenon presented here is thus very different from the perfect absorption caused by hyperbolic phonon polaritons in hBN [31], where both hyperbolicities can result in high absorption.

Considering that absorption requires a slow-light effect, one can engineer the absorption band by designing the shape of the trapezoid. An example is shown in Figure 6, where only the upper half, middle part, or the lower half of the trapezoid of the structure in Figure 2 is present in each case with h = 5 μm and Λ = 3 μm. The trapezoid is divided into 50 layers in the z-direction using a stairwise discretization. The solid line represents the absorptance in the case for 0.04 μm < t < 1 μm (upper half). Such a shape can support the slow-light effect for 6.22 μm < λ < 6.63 μm. The middle part or the lower half of the trapezoid supports the slow-light effect for regions with 6.36 μm < λ < 7.06 μm and 6.63 μm < λ < 7.29 μm, respectively. Figure 6 suggests that broadband perfect absorption may be engineered in the desired wavelength range and, moreover, the range may be extended from the ultraviolet to microwave regions by tailoring the geometry parameters of the trapezoid using suitable natural type II hyperbolic materials [28]. Note that the high absorptance peak at 6.2 μm is at the edge of the hyperbolic region, where $\varepsilon'_{\perp}$ goes from positive to negative across zero as the wavelength becomes longer. Thus, the absorption peak is presumably caused by an epsilon-near-zero effect [36] that is not related to the mechanism discussed here.

The substrate of the structure can affect the radiative properties of the structures at the wavelengths at which the slow light effect is not supported. Figure 7 shows the reflectance

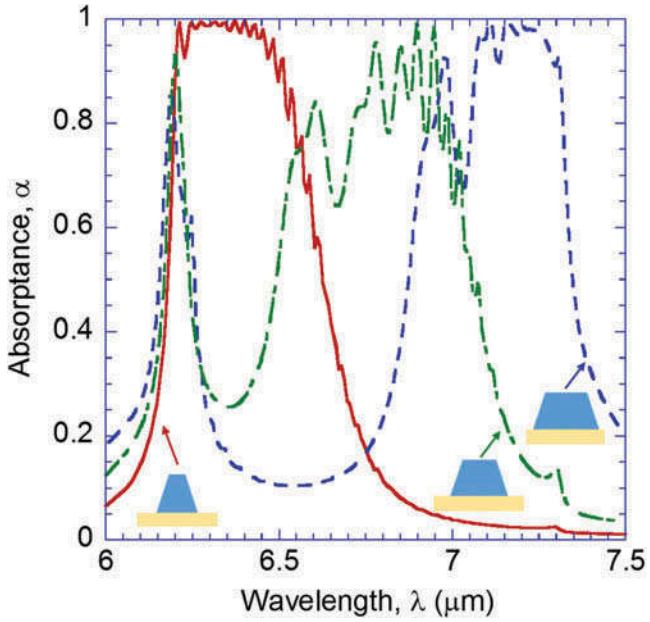

Figure 6. Absorptance spectrum of trapezoidal gratings when only the upper half, middle part, or lower half of the trapezoid in Figure 1 is present: The solid line represents the case where t_t = 0.04 μm and t_b = 1 μm (upper half); the dash-dot line is with t_t = 0.5 μm and t_b = 1.5 μm (middle part); and the dashed line is when t_t = 1 μm and t_b = 2 μm (lower half). For all cases, h = 5 μm and Λ = 3 μm.

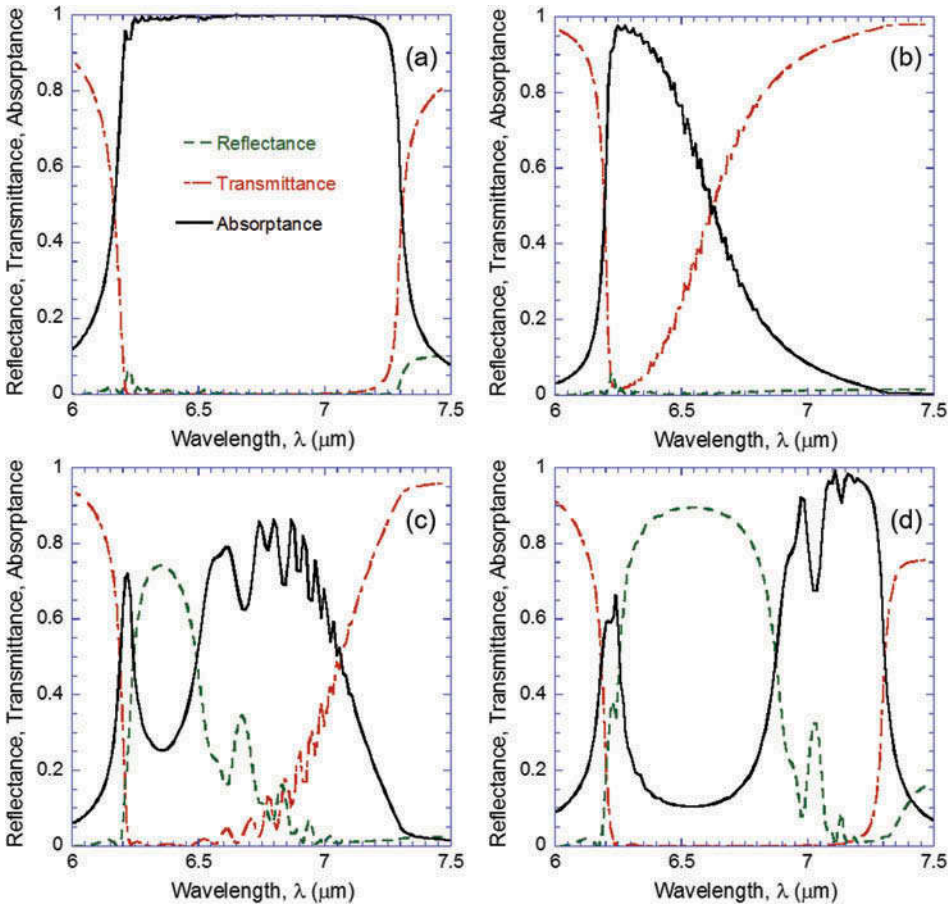

Figure 7. Reflectance (dashed line), transmittance (dot-dashed line), and absorptance (solid line) for TM waves at normal incidence ($\theta = 0°$) of four difference hBN trapezoid gratings suspended in vacuum: (a) a grating the same geometries as the structure in Figure 2; (b) only the upper half is present; (c) only the middle part is present; and (d) only the lower half is present.

(dashed line), transmittance (dot-dashed line), and absorptance (solid line) for TM waves for four different suspended gratings without a metal substrate. Figure 7a corresponds to a suspended hBN trapezoid grating in vacuum with the same grating geometries as the structure in Figure 2 without the substrate. It can be seen that the substrate plays little role on the absorptance spectrum, and the transmission is essentially zero, indicating a broadband antireflection effect. Thus, different materials other than Ag may be used as a substrate in real fabrications. Additionally, if only the upper half is present, the suspended grating can still support wavelength-selective high absorptance for short wavelengths where the slow-light effect is present, as shown in Figure 7b. Similar effects can be seen in Figures 7c and 7d as well, where only the middle and lower parts of the trapezoid are present, respectively. As the wavelength increases, the transmittance increases gradually but the reflectance does not change significantly. This can be understood because when t is small, the incident waves, regardless of wavelength, can enter the grating region without being reflected due to impedance matching. However, the transmittance is high for longer wavelengths because there is no slow-light effect to trap the energy inside the grating. Similar effects can be seen in Figure 7c as well. Therefore, a metal substrate, if present, can reflect these waves back and increase the reflectance, as indicated by Figure 6. When only the middle part is present, the reflectance of the short wavelengths increased as shown in Figure 7c.

This is because the incident waves of short wavelengths are difficult to couple with the fundamental waveguide mode in the hBN trapezoid and thus are reflected due to poor impedance matching. A similar phenomena can be seen in Figure 7d when only the lower half is present. This effect also exists in the structures with a substrate as shown in Figure 6. The absorption peaks presumably caused by the epsilon-near-zero effect shows up for all cases.

Conclusions

In conclusion, this work demonstrates that trapezoidal gratings made of materials that possess an intrinsic type II hyperbolic region can yield broadband perfect absorption. The mechanism is attributed to a slow-light effect in hyperbolic waveguides, along with the impedance matching condition. The absorption is nearly omnidirectional, and the absorption bandwidth, as well as the spectral range, can be engineered by the shapes of the trapezoid. The substrate can increase the reflectance of the wavelengths that can enter the grating region but not be halted by the slow-light effect. These findings may facilitate the usage of available natural hyperbolic materials to achieve broadband absorption, which can benefit a wide variety of applications including solar–thermal conversion, radiative cooling, and photodetection.

Funding

This research was supported by the National Science Foundation (CBET-1603761).

References

1. N.I. Landy, S. Sajuyigbe, J.J. Mock, D.R. Smith, and W.J. Padilla, Perfect Metamaterial Absorber, *Physical Review Letters*, Vol. 100, p. 207402, 2008.
2. H.-T. Chen, Interference Theory of Metamaterial Perfect Absorbers, *Optics Express*, Vol. 20, pp. 7165–7172, 2012.
3. X. Liu, T. Starr, A.F. Starr, and W.J. Padilla, Infrared Spatial and Frequency Selective Metamaterial with Near-Unity Absorbance, *Physical Review Letters*, Vol. 104, p. 207403, 2010.
4. R. Alaee, M. Farhat, C. Rockstuhl, and F. Lederer, A Perfect Absorber Made of a Graphene Micro-Ribbon Metamaterial, *Optics Express*, Vol. 20, pp. 28017–28024, 2012.
5. W. Li and J. Valentine, Metamaterial Perfect Absorber Based Hot Electron Photodetection, *Nano Letters*, Vol. 14, pp. 3510–3514, 2014.
6. B. Zhao and Z.M. Zhang, Strong Plasmonic Coupling between Graphene Ribbon Array and Metal Gratings, *ACS Photonics*, Vol. 2, pp. 1611–1618, 2015.
7. B. Zhao, L.P. Wang, Y. Shuai, and Z.M. Zhang, Thermophotovoltaic Emitters Based on a Two-Dimensional Grating/Thin-Film Nanostructure, *Interntaional Journal of Heat and Mass Transfer*, Vol. 67, pp. 637–645, 2013.
8. X. Xiong, S.-C. Jiang, Y.-H. Hu, R.-W. Peng, and M. Wang, Structured Metal Film as a Perfect Absorber, *Advanced Materials*, Vol. 25, pp. 3994–4000, 2013.
9. G. Ni, G. Li, S.V. Boriskina, H. Li, W. Yang, T. Zhang, and G. Chen, Steam Generation under One Sun Enabled by a Floating Structure with Thermal Concentration, *Nature Energy*, Vol. 1, p. 16126, 2016.
10. L. Zhou, Y. Tan, J. Wang, W. Xu, Y. Yuan, W. Cai, S. Zhu, and J. Zhu, 3D Self-Assembly of Aluminium Nanoparticles for Plasmon-Enhanced Solar Desalination, *Nature Photonics*, Vol. 10, pp. 393–398, 2016.
11. Y.-B. Chen and Z.M. Zhang, Design of Tungsten Complex Gratings for Thermophotovoltaic Radiators, *Optics Communications*, Vol. 269, pp. 411–417, 2007.
12. H. Wang and L.P. Wang, Perfect Selective Metamaterial Solar Absorbers, *Optics Express*, Vol. 21, pp. A1078–A1093, 2013.
13. A.K. Azad, W.J.M. Kort-Kamp, M. Sykora, N.R. Weisse-Bernstein, T.S. Luk, A.J. Taylor, D.A.R. Dalvit, and H.-T. Chen, Metasurface Broadband Solar Absorber, *Scientific Reports*, Vol. 6, p. 20347, 2016.
14. R. Feng, J. Qiu, L. Liu, W. Ding, and L. Chen, Parallel LC Circuit Model for Multi-Band Absorption and Preliminary Design of Radiative Cooling, *Optics Express*, Vol. 22, pp. A1713–A1724, 2014.
15. Z.H. Jiang, S. Yun, F. Toor, D.H. Werner, and T.S. Mayer, Conformal Dual-Band Near-Perfectly Absorbing Mid-Infrared Metamaterial Coating, *ACS Nano*, Vol. 5, pp. 4641–4647, 2011.
16. X. Li, W.C.H. Choy, H. Lu, W.E.I. Sha, and A.H.P. Ho, Efficiency Enhancement of Organic Solar Cells by Using Shape-Dependent Broadband Plasmonic Absorption in Metallic Nanoparticles, *Advanced Functional Materials*, Vol. 23, pp. 2728–2735, 2013.

17. W.-B. Shi, R.-H. Fan, K. Zhang, D.-H. Xu, X. Xiong, R.-W. Peng, and M. Wang, Broadband Light Trapping and Absorption of Thin-Film Silicon Sandwiched by Trapezoidal Surface and Silver Grating, *Journal of Applied Physics*, Vol. 117, p. 065104, 2015.
18. J. Zhu, Z. Yu, S. Fan, and Y. Cui, Nanostructured Photon Management for High Performance Solar Cells, *Materials Science and Engineering: R: Reports*, Vol. 70, pp. 330–340, 2010.
19. L. Tsakalakos, J. Balch, J. Fronheiser, M.-Y. Shih, S.F. LeBoeuf, M. Pietrzykowski, P.J. Codella, B.A. Korevaar, O.V. Sulima, J. Rand, A. Davuluru, and U. Rapol, Strong Broadband Optical Absorption in Silicon Nanowire Films, *Journal of Nanophotonics*, Vol. 1, p. 013552, 2007.
20. X.L. Liu, L.P. Wang, and Z.M. Zhang, Wideband Tunable Omnidirectional Infrared Absorbers Based on Doped-Silicon Nanowire Arrays, *Journal of Heat Transfer*, Vol. 135, p. 061602, 2013.
21. L. Ferrari, C. Wu, D. Lepage, X. Zhang, and Z. Liu, Hyperbolic Metamaterials and Their Applications, *Progress in Quantum Electronics*, Vol. 40, pp. 1–40, 2015.
22. H.N.S. Krishnamoorthy, Z. Jacob, E. Narimanov, I. Kretzschmar, and V.M. Menon, Topological Transitions in Metamaterials, *Science*, Vol. 336, pp. 205–209, 2012.
23. Y. Cui, K.H. Fung, J. Xu, H. Ma, Y. Jin, S. He, and N.X. Fang, Ultrabroadband Light Absorption by a Sawtooth Anisotropic Metamaterial Slab, *Nano Letters*, Vol. 12, pp. 1443–1447, 2012.
24. H. Hu, D. Ji, X. Zeng, K. Liu, and Q. Gan, Rainbow Trapping in Hyperbolic Metamaterial Waveguide, *Scientific Reports*, Vol. 3, p. 1249, 2013.
25. J. Wu, Broadband Light Absorption by Tapered Metal-Dielectric Multilayered Grating Structures, *Optics Communications*, Vol. 365, pp. 93–98, 2016.
26. X. Yang, J. Yao, J. Rho, X. Yin, and X. Zhang, Experimental Realization of Three-Dimensional Indefinite Cavities at the Nanoscale with Anomalous Scaling Laws, *Nature Photonics*, Vol. 6, pp. 450–454, 2012.
27. J. Zhou, A.F. Kaplan, L. Chen, and L.J. Guo, Experiment and Theory of the Broadband Absorption by a Tapered Hyperbolic Metamaterial Array, *ACS Photonics*, Vol. 1, pp. 618–624, 2014.
28. E.E. Narimanov and A.V. Kildishev, Metamaterials: Naturally Hyperbolic, *Nature Photonics*, Vol. 9, pp. 214–216, 2015.
29. Z.M. Zhang, *Nano/Microscale Heat Transfer*, McGraw-Hill, New York, 2007.
30. A. Kumar, T. Low, K.H. Fung, P. Avouris, and N.X. Fang, Tunable Light–Matter Interaction and the Role of Hyperbolicity in Graphene–hBN System, *Nano Letters*, Vol. 15, pp. 3172–3180, 2015.
31. B. Zhao and Z.M. Zhang, Perfect Mid-Infrared Absorption by Hybrid Phonon–Plasmon Polaritons in hBN/Metal-Grating Anisotropic Structures, *International Journal of Heat and Mass Transfer*, Vol. 106, pp. 1025–1034, 2017.
32. P. Li, B. Liu, Y. Ni, K.K. Liew, J. Sze, S. Chen, and S. Shen, Large-Scale Nanophotonic Solar Selective Absorbers for High-Efficiency Solar Thermal Energy Conversion, *Advanced Materials*, Vol. 27, pp. 4585–4591, 2015.
33. J.D. Caldwell, A.V. Kretinin, Y. Chen, V. Giannini, M.M. Fogler, Y. Francescato, C.T. Ellis, J.G. Tischler, C.R. Woods, A.J. Giles, M. Hong, K. Watanabe, T. Taniguchi, S.A. Maier, and K.S. Novoselov, Sub-Diffractional Volume-Confined Polaritons in the Natural Hyperbolic Material Hexagonal Boron Nitride, *Nature Communications*, Vol. 5, p. 5221, 2014.
34. A.J. Giles, S. Dai, O.J. Glembocki, A.V. Kretinin, Z. Sun, C.T. Ellis, J.G. Tischler, T. Taniguchi, K. Watanabe, M. M. Fogler, K.S. Novoselov, D.N. Basov, and J.D. Caldwell, Imaging of Anomalous Internal Reflections of Hyperbolic Phonon–Polaritons in Hexagonal Boron Nitride, *Nano Letters*, Vol. 16, pp. 3858–3865, 2016.
35. B. Zhao, J.M. Zhao, and Z.M. Zhang, Resonance Enhanced Absorption in a Graphene Monolayer Using Deep Metal Gratings, *Journal of the Optical Society of America B*, Vol. 32, pp. 1176–1185, 2015.
36. A. Alù, M.G. Silveirinha, A. Salandrino, and N. Engheta, Epsilon-Near-Zero Metamaterials and Electromagnetic Sources: Tailoring the Radiation Phase Pattern, *Physical Review B*, Vol. 75, p. 155410, 2007.